Fatigue Life Assessment for High Pressure Diesel Injection Components with Large Residual Stresses

Elisabeth Herz[a,c], Rayk Thumser[b], Joachim Bergmann[b] and Michael Vormwald[a]

[a] Materials Mechanics Group, Technische Universität Darmstadt,
Petersenstraße 12, D-64287 Darmstadt, Germany
[b] Materials Research and Testing Institute at Bauhaus University,
Coudraystraße 9, D-99423 Weimar, Germany
[c] Robert Bosch GmbH, Postfach 30 02 40, D-70442 Stuttgart

Abstract In the present paper, an overview on investigations regarding the fatigue life of high pressure Diesel injection components is given. Specimens with a typical, yet idealized geometry have been used in the experimental analyses. A synthetic load sequence has been designed to capture typical load histories. Several approaches to predict the finite fatigue life of such components with increasing degree of sophistication, of accuracy, and of numerical expense, are presented.

1 INTRODUCTION

In order to meet economic and ecological requirements, maximum internal pressures in Diesel injection systems have been raised to above 2500 bar. Technologies like autofrettage of components considerably raising the endurance limit have made this possible. Nevertheless, the technical methods to further increase the endurance limits are somewhat exhausted. In some cases, the fatigue design of autofrettaged Diesel injection parts for finite life under variable amplitude loading will help to meet present as well as future higher requirements. Because of the extremely high overload due to autofrettage, the life estimation is a new and challenging object of research.

In previous works, only the endurance limit of autofrettaged components has been investigated [1,2,3,4, 5,6]. To this date, the reserves that lie in fatigue life design can not be exploited because, on one hand, reliable experimental data is lacking as well as, on the other hand, sufficiently precise prediction methods. The present work is intended as a first step to close this gap for Diesel injection components. Besides providing the experimental basis taking into account realistic load sequences, analytical predictions of finite fatigue life are made.

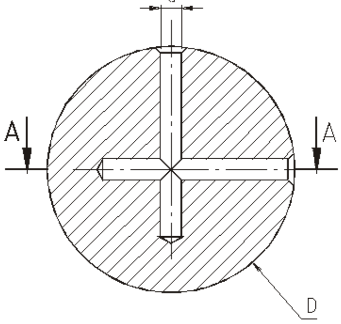

D [mm]	58
h [mm]	10
d [mm]	5
k [mm]	10
h/d	2

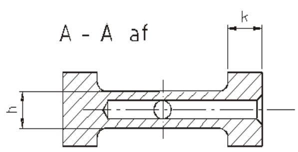

Fig. 1: Specimen geometry

2 INCIPIENT WORK

2.1 Specimen geometry and material

An experimental program has been accomplished using standardized cross bore hole specimens. Refer to fig. 1 for the specimen geometry. Tests have been performed using both non autofrettaged and autofrettaged specimens, the latter being submitted to an autofrettage pressure of p_{aut}=6000bar. For the sake of shortness, the present paper is restricted to the presentation of the results for autofrettaged specimens.

A 42CrMo4 (AISI 4140) steel with a yield strength of 875 MPa and an ultimate tensile strength of 940 MPa has been employed. In order to determine the stress strain behaviour of the material, cyclic axial tension-compression tests have been performed on LCF specimens. The results of the first loading and unloading from various maximum strains are shown in fig. 2. The material behaviour can be described by the plasticity model according to Döring [7]. For the finite element calculations of the residual stresses due to autofrettage and the level 4 crack growth simulations (see sections 3 and 4.2.3), a parameter set for this plasticity model has been determined by a curve fit. The stress-strain curves calculated using the model are included in fig. 2.

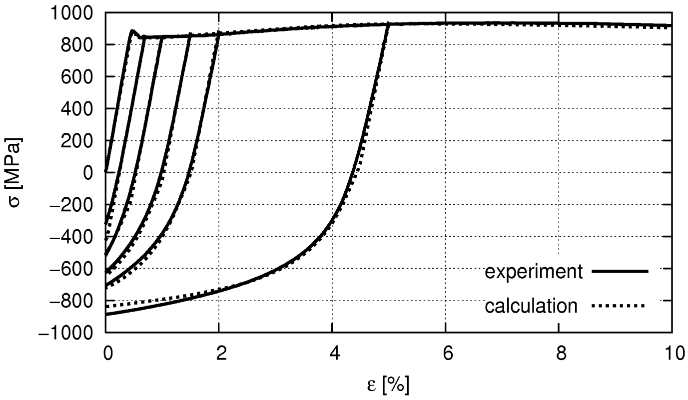

Fig. 2: Material behaviour, experiment and calculation

2.2 Synthetic load sequence CORAL

Based on measured typical common rail load data, a synthetic load sequence has been designed and named CORAL – **CO**mmon **RA**il **L**oad sequence. Very small load cycles with a range of less than 10 % of the maximum range are omitted. The sequence consists thus of 3 million load cycles in total including 30 000 start stop cycles, see fig. 3.

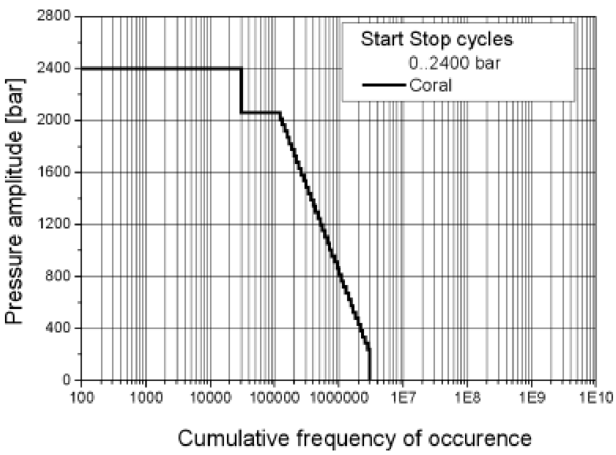

Fig. 3: Histogram of the CORAL sequence for an exemplary maximum pressure of 2400bar

3 RESIDUAL STRESS CALCULATION

The beneficial effect of autofrettage on fatigue life is caused by the introduced compressive residual stresses. The accuracy of any fatigue life prediction method is thus crucially influenced by the accuracy of their determination of the residual stresses. This strongly depends on a realistic description of the material behaviour on one hand, and the threedimensional geometry, on the other hand. Therefore, residual stresses are calculated using a finite element model (see section 4.2.3) and the plasticity model mentioned in section 2.1. In fig 4, the resulting residual stress distribution along the bisector between the bore holes is displayed.

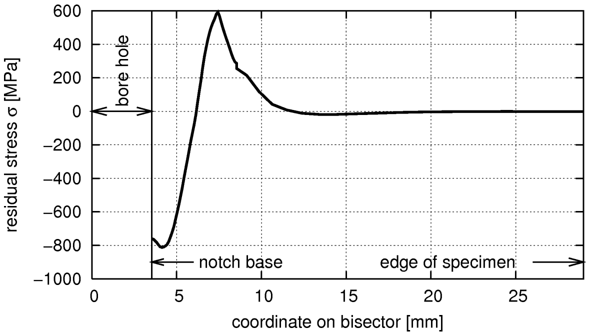

Fig. 4: Residual stress distribution along the bisector between the bore holes, normal stress component perpendicular to the plane of fatigue crack growth

4 FATIGUE LIFE ANALYSES

4.1 Nominal stress approach (Level 1)

In the first level, the applicability of common design rules as e.g. recommended in [8,9] is investigated. These are based on S-N-curves and a Miner-type damage accumulation and take into account influences of shape, size, surface, etc. For autofrettaged components, the crack growth is significantly hampered by the residual stress field. That is why a basic S-N-curve on the basis of uncracked material data cannot lead to satisfying results. Thus, experimentally determined component S-N-curves are chosen as a point of origin.

The influence of the mean stress is taken into account by applying a criterion formally equivalent to the damage parameter P_{SWT} [10]. In fig. 5 a), the resulting mean stress influence is illustrated in the form of a Haigh diagram. Furthermore, a basic S-N-curve is needed to determine the cycles to failure. Fig. 5 b) shows the experimentally determined curve for $R \approx 0$. In the area of small load ranges, a significant decrease in the slope can be stated. This is due to the favourable influence of the autofrettage residual stresses. The basic S-N-curve is fitted to the upper slope in order to be conservative. As is illustrated in fig. 5 b), the S-N-curve is prolonged as a straight line below the endurance limit in order to take into account the damage caused by small load cycles. Load sequence effects other than those due to small cycles are not considered. The Miner damage sum is set to D=1 at failure.

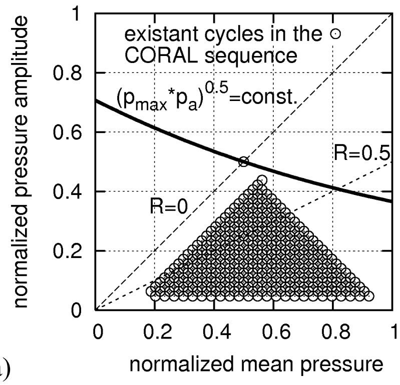

a)

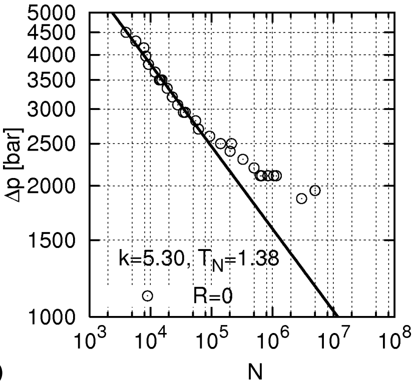

b)

Fig. 5: a) Haigh-diagram with rainflow-counted cycles of the CORAL load sequence, b) basic S-N-curve

4.2 Fracture mechanics based approaches

Three more approaches with increasing levels of sophistication have been investigated. These aim at calculating crack growth by means of fracture mechanics. Herein, the consideration of residual stresses is of outstanding importance. While the second level is restricted to linear elastic fracture mechanics, the third as well as the fourth level are based on elastoplastic fracture mechanics.

4.2.1 Level 2 – Linear elastic fracture mechanics

In the second level, residual stresses are treated as mean stresses modifying the mean value of the stress intensity factor, the range of which is determined by the pressure range. The weight function of Oore and Burns [11] for a general internal crack (see fig. 6 a) is generalized to surface cracks. With a sufficiently fine meshing of the crack front (see fig. 6 b), a very good agreement between numerically and analytically determined stress intensity factors is achieved. This approach allows for the simulation of varying crack front shapes during the crack growth process. This detail is not considered by either of the other levels. However, the approach neglects effects from nonlinear material behaviour.

a) 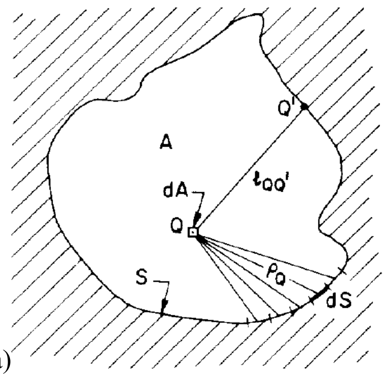

b) 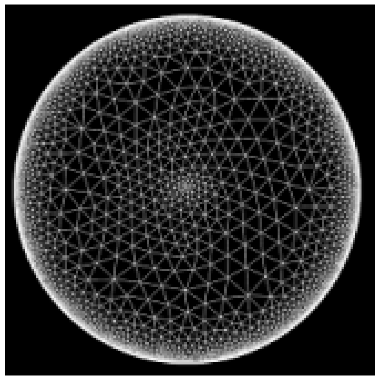

Fig. 6: a) General two dimensional internal crack, b) meshing of circular internal crack

4.2.2 Level 3 – Crack growth simulation with an extended strip yield model

In the level 3 and 4 approach, it is assumed that crack growth starts from an initial length of 250µm. Technical crack initiation up to this crack length is calculated by means of the local strain approach employing the damage parameter P_{SWT} [10]. The crack has to traverse the compressive residual stress field built up by autofrettage. Crack growth is driven by the effective stress ranges between crack opening pressure and maximum pressure, see fig. 7. The crack is able to grow according to a Paris law only if these effective pressure ranges result in larger ranges of the effective stress intensity factor than the respective threshold, see eq. (1).

$$\frac{\mathrm{d}a}{\mathrm{d}n} = 1.37 \cdot 10^{-8} \frac{\mathrm{mm}}{\mathrm{cyc}} \cdot \left(\frac{\Delta K_{\mathrm{eff}}}{\mathrm{MPa}\sqrt{\mathrm{m}}} \right)^3 \quad \text{for} \quad \Delta K_{\mathrm{eff}} > \Delta K_{\mathrm{eff,th}} = 3\ \mathrm{MPa}\sqrt{\mathrm{m}} \qquad (1)$$

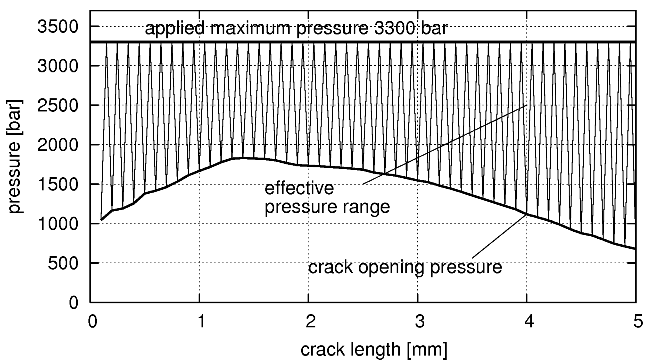

Fig. 7: Crack opening pressures and effective pressure ranges (example)

In level 3, the effective pressure ranges are determined by means of the well established Newman model [12,13], which has been developed based on the Dugdale model. The real component geometry is replaced by a two-dimensional middle crack plate. The crack face as well as the ligament are discretized in strips that follow an ideally plastic material law. While this model can already inherently capture crack closure and plasticity effects, it has now been enhanced to accept residual stresses determined by other methods as an initial condition. Here, the residual stresses along the bisector calculated with the finite element method (see section 3) have been taken as an initial condition. The two free parameters of the Newman model, i.e. the yield stress σ_f, and the multiaxiality parameter α, have been fitted so that the endurance limit can correctly be determined. It was found that a choice of σ_f equal to the stabilized cyclic 0.2% proportionality limit $R'_{p0.2}$ and $\alpha = 3$ (high multiaxiality) leads to satisfyingly accurate results when calculating constant amplitude S-N-curves (see fig. 10).

The accuracy of crack growth calculations under service loads can significantly be increased by taking into account load sequence effects. These effects can most naturally be captured by applying variable amplitude load sequences to a Newman strip yield model. Nevertheless, in order to reduce numerical expenses, the procedure used to this aim had to be designed to be as effective as possible. This has been achieved by seperating the integration of the Paris law from the crack growth simulation. The procedure proves to be appropriate to determine crack opening stresses taking into account load sequence dependent residual stress redistributions. Thus, the effective load ranges dominating crack growth are accessible with high accuracy, and satisfying predictions of finite fatigue life results can be made (see fig. 11).

4.2.3 Level 4 – explicit crack growth simulation with finite elements

Level 4 is the most sophisticated of the presented approaches. Here, a finite element crack growth simulation is performed. The plasticity model accordign to Döring [7] has been used. With this constitutive model, mean stress relaxation and ratchetting can be simulated which especially near the crack tip strongly influence the crack opening and closure behaviour. Moreover, the basically three dimensional stress-strain-state in the specimen can be taken into account.

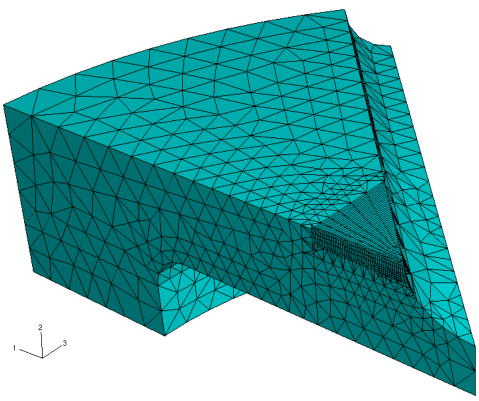

a)

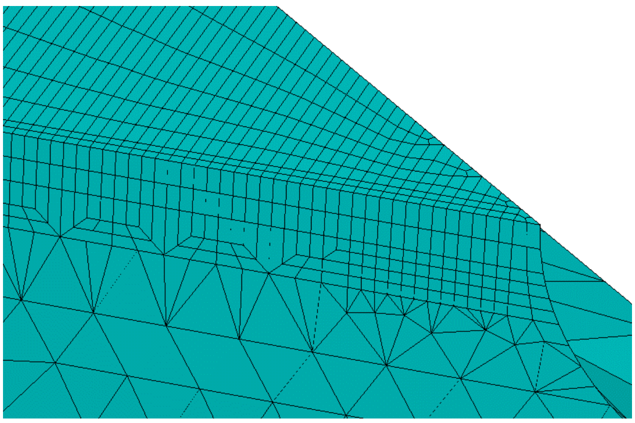

b)

Fig. 8: a) Finite element model, b) refined section at the notch

In level 4, the effective pressure ranges have thus been calculated by extensive finite element calculations, using ABAQUS and the aforementioned constitutive model linked by UMAT interface. The specimen is modelled fully three-dimensionally, taking into account all symmetry axes. The modelling accuracy is only limited by the assumption that the crack front is a straight line perpendicular to the bisecting line between the boreholes. In the case of autofrettaged components, this assumption is supported by experimental findings.

Convergence studies yielded that for the here investigated autofrettaged specimens and applied pressures, an element size of 100µm is sufficiently small to achieve converged solutions. As outlined in [5, 6], the simulation was performed in several steps:

- Loading the specimens by autofrettage pressure and unloading to 50 bar (minimum pressure in cyclic test), see section 3
- 250 cycles at $\Delta p_{service}$ for stress redistribution in the whole component
- Simulating crack propagation in 100 µm steps

- In each step stabilizing mean stress ahead of crack tip by applying a small number of cycles
- Determine crack closure and opening level along the bisecting line

By this simulation, effective pressure ranges have been determined. This procedure has been validated in several previous works dealing with the determination of the endurance strength of components. The procedure has now been modified and enhanced to deal with the case of variable amplitude loading. Due to the numerical limitations, it is to this date impossible to subject a finely meshed finite element model of a component to a real load sequence with up to several million load cycles, most of them causing plastic deformations. Nevertheless, it is indispensible to correctly model load sequence effects. Otherwise, the high accuracy of the here presented highly sophisticated approach would be lost.

Therefore, a set of curves of crack opening pressures is calculated depending on current as well as previous loading ranges and R ratios. In fig. 9, a selection of crack opening pressures relative to crack length is, for the sake of clarity plotted in two graphs. Load sequence effects can be observed in the results of the finite element calculation: In fig. 9 a), the curves resulting for a load cycle preceded by smaller cycles are plotted. These curves significantly differ from those in fig. 9 b), where results for the same load ranges preceded by a larger load cycle are displayed. A more detailed consideration of the load sequence effects is not possible because further refinement of the mesh would have gone beyond the bonds of computer storage and time.

Based on these curves of effective pressure ranges, crack propagation is calculated by means of the Paris law, eq (1). The stress intensity factors that are also determined by finite element simulation assuming linear elastic material behaviour.

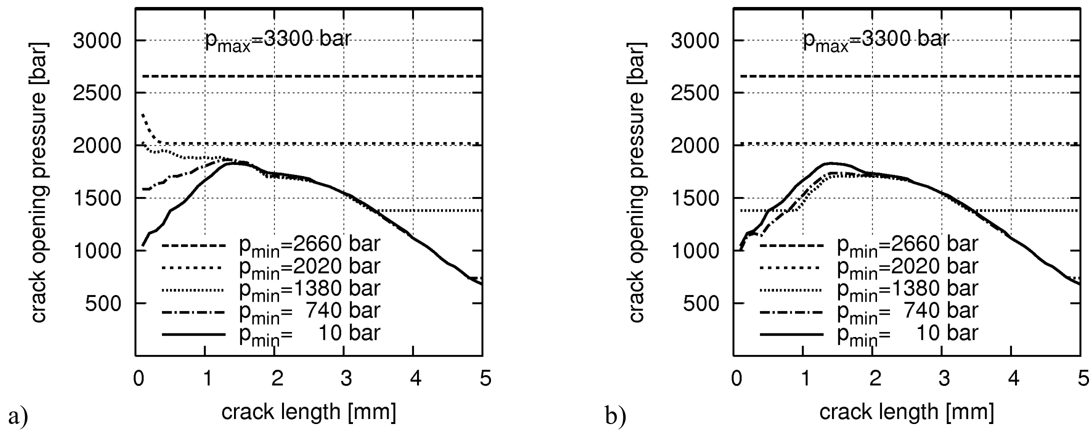

Fig. 9: Selection of some crack opening pressure curves, a) following a smaller cycle, b) following a larger cycle

5 RESULTS OF FINITE FATIGUE LIFE CALCULATIONS

In fig. 10, the constant amplitude S-N-curves as calculated with level 3 and 4 approaches are compared to the experimental results. A very good agreement is achieved in both cases.

In fig. 11, the experimental results of the variable amplitude loading tests are plotted in comparison to the constant amplitude tests at a load ratio of approximately 0. Additionally, the computation results are displayed. Unfortunately, results from level 2 can not yet be provided. It can be stated that, regarding the high simplicity of the approach, the accuracy achieved by level 1 is satisfying. Nevertheless, fatigue life is underestimated at pressure levels in the vicinity of the endurance limit, i.e. in the region where fatigue life design might be promising. The overestimation of fatigue life, that the nominal stress approach is yielding at higher pressure levels, (approximately factor 2) is mainly due to the insufficient consideration of load sequence effects.

The two curves describing the fatigue lives as computed by the two elastoplastic fracture mechanics based approaches show a significantly better agreement with the experimental results. It is especially promising that with these two methods, the decrease of the S-N-curve slope in the region of lower pressures can be captured. The slight overestimation of fatigue lives is mainly due to the fact that long crack growth life as it is calculated with these methods is assumed to start only at an initial crack length of 250 µm. The part of life up to this crack length is calculated using P_{SWT} damage parameter, neglecting load sequence effects.

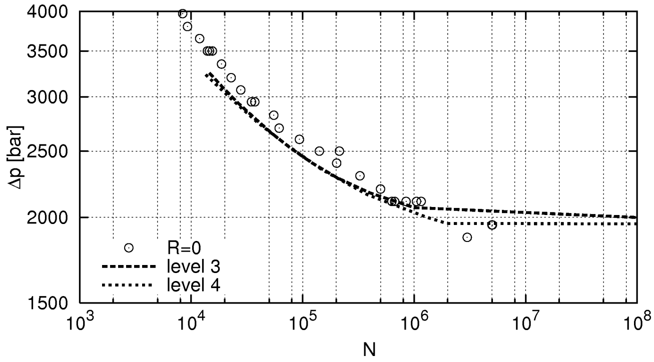

Fig. 10: S-N-curves

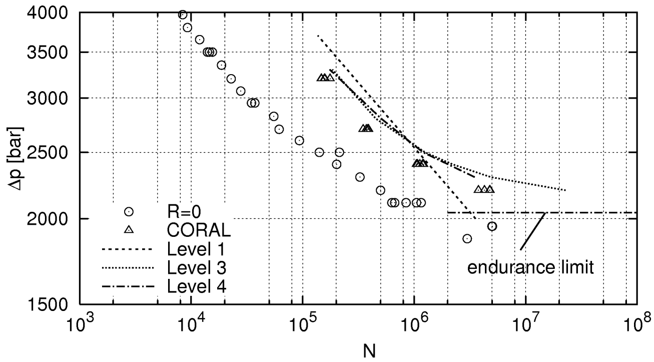

Fig. 11: Results of fatigue life calculations

Between the levels, there is always more than one order of magnitude in computer time. In this case, it took about 24 hours to calculate the fatigue life curve with level 3, while level 4 calculations took several weeks. Thus, it may be very promising to recommend level 3 approach for future research. Nevertheless, it should be noted that these good results are only possible when the residual stress distribution has been determined with an accurate finite element calculation.

6 CONCLUSIONS

In the present paper, an overview has been given over the vast experimental and analytical work done to capture fatigue life of autofrettaged components under variable amplitude loading using a synthetical load sequence that has been created based on typical common rail load data.

Four simulation methods have been introduced for the calculation of finite fatigue lives. Besides the state-of-the-art nominal stress approach used with an appropriate mean stress criterion and the elementary Miner rule, three fracture mechanics based approaches have been established. Special emphasis has been laid on the third and fourth level that take into account plastic material behaviour. On one hand, this is the Newman strip yield model that has been enhanced to incorporate finite element calculated residual stress distributions, and an even more complex method involving the application of a plasticity model able to accurately describe all relevant deformation characteristics and a finite element based crack propagation calculation. Both methods yield crack opening pressures and effective ranges of the stress intensity factor. Based on these, fatigue lives are calculated using the Paris law.

Especially with these two levels, a good agreement with the experimental results can be achieved, although lying slightly on the unsafe side. It can thus be concluded that fatigue life design can lead to higher admissible pressures. In the present paper, only mean values are given. It is to be expected that the beneficial effect of autofrettage is amplified by the smaller scatter of experimental finite fatigue life data leading to smaller necessary safety factors.

The presented methods all prove appropriate for the further development of a finite fatigue life prediction. The more sophisticated methods have – additionally to being more accurate – the advantage of needing far less experimental data while, on the other hand, consuming significantly more computational resources. However, especially the Newman strip yield model seems to be a promising way to reconcile the need for accuracy and efficiency, respectively.

7 ACKNOWLEDGEMENT

The authors gratefully acknowledge the financial support provided by the Forschungsvereinigung Verbrennungskraftmaschinen e. V. (FVV) and Arbeitsgemeinschaft industrieller Forschungsvereinigung “Otto von Guericke” (AIF) under contract FVV 608 802. Support of the FVV working group “Autofrettage” is thankfully appreciated.

8 REFERENCES

1. Seeger, T., M. Schön, J. Bergmann, and M. Vormwald, *Autofrettage I: Vorhaben Nr. 478; Dauerfestigkeitssteigerung durch Autofrettage; Abschlussbericht;* . 1994, Frankfurt: Forschungsvereinigung Verbrennungskraftmaschinen e. V. (FVV).

2. Seeger, T., S. Greuling, and J.W. Bergmann, *Autofrettage II: Vorhaben Nr. 671; Dauerfestigkeitssteigerung durch Autofrettage II; Abschlußbericht; Heft 704*. 2001, Frankfurt: Forschungsvereinigung Verbrennungskraftmaschinen e. V. (FVV).

3. Thumser, R., J.W. Bergmann, and M. Vormwald, *Residual Stress Fields and Fatigue Analysis of Autofrettaged Parts.* International Journal of Pressure Vessels and Piping, 2001. 79(2): p. 113-117.

4. Thumser, R., et al., *Bruchmechanische Bewertung der Dauerfestigkeit von autofrettierten Diesel-Einspritzleitungen*, in *Berichtsband 36. Tagung DVM-AK Bruchvorgänge*. 2004: Köln.

5. Herz, E., R. Thumser, M. Vormwald and J. Bergmann, *Endurance Limit Design of High Pressure Diesel Injection Pipes for Low Failure Probability*. In: Proceedings of Fatigue Design 2005, Senlis 2005

6. Herz, E., R. Thumser, M. Vormwald and J. Bergmann, *Endurance limit of autofrettaged Diesel-engine injection tubes with defects*. Eng. Fract. Mech. 73 (2003), p. 3-21

7. Döring, R., et al., *A Plasticity Model for Calculating Stress-Strain Sequences under Multiaxial Nonproportional Cyclic Loading.* Computational Materials Science, 2003. 28(3-4): p. 587-596.

8. Bergmann, J. and R. Thumser, *Synthetische Wöhlerlinien für Eisenwerkstoffe*, Studiengesellschaft Stahlanwendung e.V., 1999, Düsseldorf

9. Hänel, B., E. Haibach, T. Seeger, G. Wirthgen, and H. Zenner, *FKM - Guideline, Analytical Strength Assessment,* 5th edition, VDMA Verlag, Forschungskuratorium Maschinenbau, Frankfurt, 2003

10. K.N. Smith, P. Watson, T.H. Topper, *A Stress-Strain Function for Fatigue of Metals*, Journal of Materials, IMLSA, 1970, Vol 5, p. 767-778

11. Oore, M. and D.J. Burns, *Estimation of Stress Intensity Factors for Embedded Irregular Cracks Subjected to Arbitrary Normal Stress Fields*. Journal of Pressure Vessel Technology, 102, p. 202-211, 1980

12. Newman, J.C., Jr., *A Crack -Closure Model for Predicting Fatigue Crack Growth Under Aircraft Spectrum Loading*. In: ASTM STP 748, p. 53-84

13. Newman, J.C., Jr., *A Crack Opening Stress Equation for Fatigue Crack Growth.* In: International Journal of Fracture, 1984, p. 131-135